A&A 465, 1021–1034 (2007)
DOI: 10.1051/0004-6361:20065421

Astronomy & Astrophysics

Investigation of long-duration arcade flares

I. Morphology and physical parameters

S. Kołomański

Instytut Astronomiczny Uniwersytetu Wrocławskiego, Kopernika 11, 51-622 Wrocław, Poland
e-mail: kolomans@astro.uni.wroc.pl

Received 12 April 2006 / Accepted 23 January 2007

ABSTRACT

Aims. We present the analysis of the three well-observed long-duration arcade flares (LDAFs). We aim to find general properties of LDAFs. In this paper results concerning morphology and physical parameters in these flares are shown.
Methods. *Yohkoh* observations, Kitt Peak Vacuum Telescope (KPVT) magnetograms and *GOES*/SEM measurements are used to determine morphology and evolution of the analysed flares and physical parameters of their loop-top kernels (temperature, density, altitude).
Results. We found that: (1) a so-called arcade channel may exist in LDAFs; (2) the energy release in LDAFs occurs in several places simultaneously and the reconnection process is not uniform along the flaring arcade; (3) a presence of 20−30 MK hot plasma during the decay phase suggests that the reconnection occurs after the LDAF maximum.

Key words. Sun: corona – Sun: flares – Sun: X-rays, gamma rays

1. Introduction

Long-duration events (LDEs) are a type of solar flares. LDEs are characterized by a slow decrease in brightness as seen in soft X-rays (SXR). This decrease (the so-called decay phase) lasts from several hours to more than a day. Much progress in studying LDEs was made by satellite observations in the ultraviolet and X-rays, such as those made during *Skylab*, *SMM* (Solar Maximum Mission) and *Yohkoh* space missions.

X-ray and ultraviolet observations taken from the *Skylab* space station showed that most LDEs occur in arcades of loops. This type of LDE we call long-duration arcade flares (LDAFs). A typical LDAF consists of several loops which form an arcade with bright emission kernels placed at the tops of the loops (loop-top kernels). The analysis of SXR images indicates that the kernels may be connected by a magnetic tube (the so-called arcade channel; see Tomczak 1994; Jakimiec et al. 1997). Investigation of these flares, carried out by many authors using X-ray images from *Skylab*, led to several important conclusions (see Sheeley et al. 1975; Vorpahl et al. 1977; Kahler et al. 1977):

1. LDAFs more frequently occur in older active regions.
2. They are large expanding structures – sometimes their height reaches almost 10^5 km. Expansion rates of arcades are typically of the order of 1 km s^{-1}.
3. A "linear structure" running along the tops of loops is the brightest part of arcade. More detailed investigation of *Skylab* images showed that this structure consists of "bright knots". The knots are called loop-top (flare) kernels or loop-top sources.
4. The kernels are the hottest and densest part of the arcade. A detailed analysis showed that there must be a continuous energy release during the whole flare evolution. If not, the kernels would disappear within minutes due to conductive and radiative losses. Moreover, observations and numerical simulations suggested that some restrictions to a flow of mass and energy out of the kernels to loops "legs" must exist.

Observations of solar flares from the *Skylab* space station were made from May 1973 to February 1974 and the observational material is rather meagre. Furthermore, the observations were recorded on film, which is worse detector than the CCD cameras used nowadays. Thus, although a significant progress in the study of LDAFs was possible owing to the *Skylab* observations, many questions remained unanswered.

Observations made by the Japanese satellite *Yohkoh* during over 10 years of operation were the next large step in the study of these flares. The satellite gave solar physicists an enormous amount of solar flares observations. Excellent *Yohkoh* light curves, spectra and images enabled the study of LDAFs in detail. Investigations carried out by many authors (e.g. Tsuneta et al. 1992; Feldman et al. 1995; Tomczak 1997; Harra-Murnion et al. 1998; Isobe et al. 2002) have confirmed results obtained from *Skylab* concerning LDAF morphology and physical parameter distributions. The investigations also indicated that continuous energy release must exist during the LDAF decay-phase to ensure the long duration of their loop-top kernels in spite of the radiative and conductive losses. Moreover, *Yohkoh* observations allowed us to build and test theoretical models of arcade flares (e.g. Choe & Lee 1996a,b; Hirose et al. 2001; Morita et al. 2001). Interesting results concerning arcade flare morphology and evolution were obtained also from *TRACE* high resolution observations (e.g. Uchida et al. 2003).

Flare loop-top kernels were studied by many authors (e.g. Acton et al. 1992; Doschek et al. 1995; Jakimiec et al. 1998) because it appeared that the kernels are a common feature of different solar flares types (including also LDAFs). The magnetic reconnection and annihilation is a source of energy released in flares. It is considered that these processes take place

Table 1. Analysed LDAFs – data from *GOES*/SEM database.

date	beginning [UT]	duration [h]	X-ray class
7 May 1993	20:20	7	M1.6
14 May 1993	21:54	10	M4.5
27 Apr. 1998	08:55	19	X1.0

inside the kernels (Jakimiec 2002a,b) or above them (e.g. Kopp & Pneuman 1976; Shibata 1999; Hirose et al. 2001).

LDAFs have a more complicated structure than compact flares, but they last longer and are much larger. Taking temporal and angular resolution of present-day X-ray observations into account, these features of the LDAFs can help us to understand solar flares and to build a correct model of these events. Detailed analysis of LDAFs and their kernels also give us possibility to understand the reconnection process.

For our study we chose three well-observed LDAFs. We investigate:

1. morphology and evolution in soft and hard X-rays;
2. physical parameters of the loop-top kernels (temperature, emission measure, density);
3. evolution of the LDAFs loop-top kernels in the diagnostic diagrams;
4. the rate of the energy release for the LDAF decay-phase.

In this paper we concentrate on two first topics given above. In Sect. 2 the methods of analysis are described. Results of the investigation for each of the selected flares are shown in Sect. 3. Discussion and conclusions are given in Sects. 4 and 5, respectively. Results concerning energy release in LDAFs (the analysis of the energy balance and diagnostic diagrams) will be presented in a subsequent paper (Paper II).

2. Analysis

We have selected and analysed three long-duration arcade flares. These LDAFs occurred on 7 and 14 May 1993 and on 27 April 1998. Basic information about the flares is given in Table 1. In our analysis we applied observations made by the following instruments:

- *Yohkoh*/SXT (Soft X-ray Telescope; Tsuneta et al. 1991);
- *Yohkoh*/HXT (Hard X-ray Telescope; Kosugi et al. 1991);
- KPVT (Kitt Peak Vacuum Telescope; Livingston et al. 1976);
- *GOES*/SEM (Space Environment Monitor; Donnelly et al. 1977).

SXT images made with Be119, Al12 and Al.1 filters were used in the analysis. Saturated or underexposed images were rejected. Selected images were reduced using SolarSoftWare procedures.

2.1. Estimation of loop-top kernels altitudes

The altitude (h) of loop-top kernels above the photosphere helps us to understand evolution of LDAFs and is necessary for the energy balance calculation. To estimate the altitude we need to know the position of a kernel in the SXT image and find the point above which the kernel is situated (sub-kernel point). The kernel position was defined by its centroid. The centroid was calculated as a center of gravity in the sense of intensity distribution within the 70% isointensity contour (relative to the brightest pixel in the Al12 image). To locate the sub-kernel point we assumed that the analyzed kernels were situated vertically above the magnetic neutral line ($H_{\rm II} = 0$). Under such assumption the sub-kernel point lays on the neutral line. To find the location of the neutral line we utilized magnetograms from the Kitt Peak Vacuum Telescope.

The kernel altitude was calculated as the distance between its centroid and the sub-kernel point. The obtained altitudes are the real altitudes, not projected on the image plane. For each kernel the value of h was calculated for several selected moments. To compare the magnetograms with the SXT images, the magnetograms were rotated to account for the solar differential rotation. Using these altitudes we can calculate the velocity of an upward or downward movement of a kernel. The relative error of h is about 10 percent.

2.2. Temperature and emission measure

Temperature (T) and emission measure (ϵ) can be estimated using a simple method called the filter ratio method (FRM; Vaiana et al. 1973; Gerassimenko & Nolte 1978). In the method we compare the ratio of fluxes measured in two different bands with theoretical predictions. From this comparison we obtain T. Using this temperature and flux measured in one filter we can calculate ϵ.

Yohkoh/SXT observations offer large possibilities for plasma diagnostics. Using these data we can estimate T and ϵ for chosen parts of the corona (e.g. a kernel). We can also create maps of T and ϵ spatial distribution. The filter ratio method for *Yohkoh*/SXT observations is described by Hara (1992) and Hara et al. (1992).

We must remember that plasma in solar flares is not isothermal. Thus, T determined from FRM method is an average T in the considered line-of-sight part of the plasma (in one pixel or in a flare kernel) and ϵ differs slightly from the total ϵ of this plasma (Gerassimenko & Nolte 1978).

To estimate the temperature and emission measure of the analysed loop-top kernels we use SXT images in Al.1, Al12 and Be119 filters. This allowed us to determine two pairs (T, ϵ). From fluxes measured in Al.1 and Al12 (the ratio Al12/Al.1 will be called the Al12 diagnostics) we obtain $T_{\rm A}$ and $\epsilon_{\rm A}$. From Al12 and Be119 (the ratio Be119/Al12 will be called the Be119 diagnostics) – $T_{\rm B}$ and $\epsilon_{\rm B}$. We calculated temperature and emission measures for each analysed flare kernel. Kernel boundaries were always taken at $0.5 I_{\rm max}$ ($I_{\rm max}$ is the intensity of the brightest pixel in a given Al12 image). The error of estimated values of T and ϵ is about 0.1–0.4 MK and less than 0.1 dex, respectively.

Temperatures $T_{\rm A}$ and $T_{\rm B}$ estimated for the same area and time are not equal – the second one is always higher (see Hara et al. 1992). The emission measures $\epsilon_{\rm A}$ and $\epsilon_{\rm B}$ are different too, but the difference is small (comparable with the error of ϵ). The difference between $T_{\rm A}$ and $T_{\rm B}$ for the flare kernels will be discussed in detail in Sect. 4.2.

2.3. Electron density

The relation between emission measure and electron density (N) of a kernel is:

$$\epsilon = \int_V N^2 {\rm d}V, \qquad (1)$$

where V is the kernel volume. From this we obtain the mean kernel density:

$$N = \sqrt{\frac{\epsilon}{V}}. \quad (2)$$

To calculate N, we must first estimate V. Kernel boundaries, taken at $0.5I_{\max}$, were nearly elliptical as seen in SXT images. Thus, the area (S) of the kernel projected on the image plane is equal to:

$$S = \pi \frac{d_2}{2} \frac{d_1}{2}, \quad (3)$$

where d_1 and d_2 is the minor and major axis, respectively. If we assume that kernel size in the direction perpendicular to the image plane is equal to d_1, the kernel will be a spheroid and its volume is:

$$V = \frac{4}{3}\pi \frac{d_2}{2} \left(\frac{d_1}{2}\right)^2, \quad (4)$$

or, using Eq. (3):

$$V = \frac{2}{3} S d_1. \quad (5)$$

Taking S as the number of pixels within the boundary $0.5I_{\max}$ and using Eqs. (2) and (5), we can estimate the electron density in the kernel. The relative error of N is about 10−15 percent.

2.4. Observations in hard X-rays

Data from *Yohkoh*/HXT were used to estimate the hardness of flare radiation and to obtain images. The hardness was defined as the ratio (R) of fluxes measured in channels M1 and L (hardness ratio M1/L). Often hard X-ray (HXR) light curves were the superposition of two kinds of variability: slow (smooth) and rapid (impulsive). In such cases, the hardness ratio was calculated also for these two components separately.

The value of R allows us to determine whether observed emission is thermal or not. We can assume two models of HXR emission: thermal (single-temperature thermal Bremsstrahlung) or non-thermal (single-power-law non-thermal Bremsstrahlung). Assuming the first model, R can be expressed in terms of the temperature of emitting plasma. In the second case, the hardness ratio is used to the calculate spectral index γ of the power-law energy spectrum in the form:

$$f(E) \propto E^{-\gamma}, \quad (6)$$

where $f(E)$ is HXR flux measured at energy E. However we should keep in mind that, generally, the observed HXR are a sum of both kinds of emission.

HXT images were synthesized using the Maximum Entropy Method (MEM; Frieden 1972; Gull & Daniels 1978; Willingale 1981; Sakao 1994), with modulation patterns computed by Sato (Sato 1997; Sato et al. 1999). In channel L the number of counts was sufficient to obtain images for all analysed flares, in channels M1 and M2 practically only for the 14 May 1993 flare (we were able to obtain only one M1 image for the 27 April 1998 flare). Each HXT image was overlaid on the SXT/Be119 image accumulated for the same time-interval. The overlaying helps to study flare morphology. Accuracy of the coalignment is about 1 arcsec (0.5 SXT pixel).

The image synthesis from HXT data must be performed very carefully, especially when HXR emission is weak. Thus, to obtain reliable HXT images each final image was compared with control images. We used two types of control image: (1) images made for time-intervals longer and shorter than for the controlled image; (2) images made for neighbouring time-intervals. Structures in the controlled image were recognized as reliable only if they were present also in the control images.

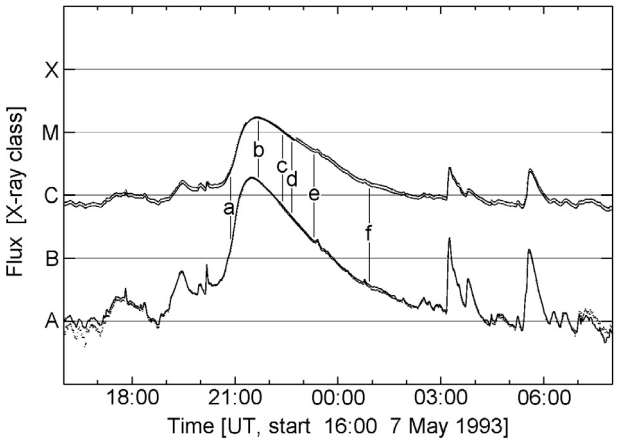

Fig. 1. *GOES*/SEM X-ray fluxes for the 7 May 1993 flare (upper curve: 1−8 Å, lower curve: 0.5−4 Å). Vertical lines indicate the observation time of the *Yohkoh*/SXT images shown in Fig. 2.

3. Results

3.1. The 7 May 1993 flare

The LDAF of 7 May 1993 occurred in the NOAA AR 7500 at N14 E41. The flare began at 20:30 UT (see Fig. 1) and reached its maximum (M1.6) 50 min later. The decay phase of the flare lasted about 6 h.

Yohkoh observations cover the whole duration of the flare. Figure 2 shows a sequence of *Yohkoh*/SXT images of the 7 May 1993 flare. Before the flare maximum, one elongated kernel (the kernel A, see Fig. 2a) was seen in the SXT images. The kernel A was connected with the footpoint E by a bright loop. At the flare maximum two new kernels (kernels B and C, see Fig. 2b) began to be seen on the opposite sides of the kernel A. After the satellite night, one can see in the SXT images three bright kernels (A, B, C) and one weak kernel D (see Fig. 2c). These kernels were situated at the top of high arcade of loops. As time passed, the kernels disappeared one after the other: the kernel A at about 23 UT, then, 30 min later, the kernel C (see Fig. 2e). The kernels B and D lasted the longest time, they disappeared after 1 UT on 8 May. When these kernels began to disappear a bright structure running along the tops of the loop became visible (see Fig. 2f).

The discussed flare clearly showed upward expansion. To study this process quantitatively, altitudes of the kernels were estimated. The results are shown in Fig. 3. The altitudes of the kernels grew during the flare evolution from about 4×10^4 km to 6×10^4 km with velocity decreasing from 2 to 0 km s^{-1}.

From SXT data we derived for each kernel its T, ϵ and N. The Al diagnostics covers the whole duration of the kernels and the Be diagnostics is available only before 22:32 UT (no Be119 images after that moment). This is why we present here only Al diagnostics results. Figure 4 shows temperature versus time for all four kernels. Temperature maximum was reached at 21:10 UT (8.5 MK, the kernel A) and after that T of all kernels decreased. At 1:00 UT on 8 May the kernels B and D had T of only about 6.1 MK. There was an interesting situation after

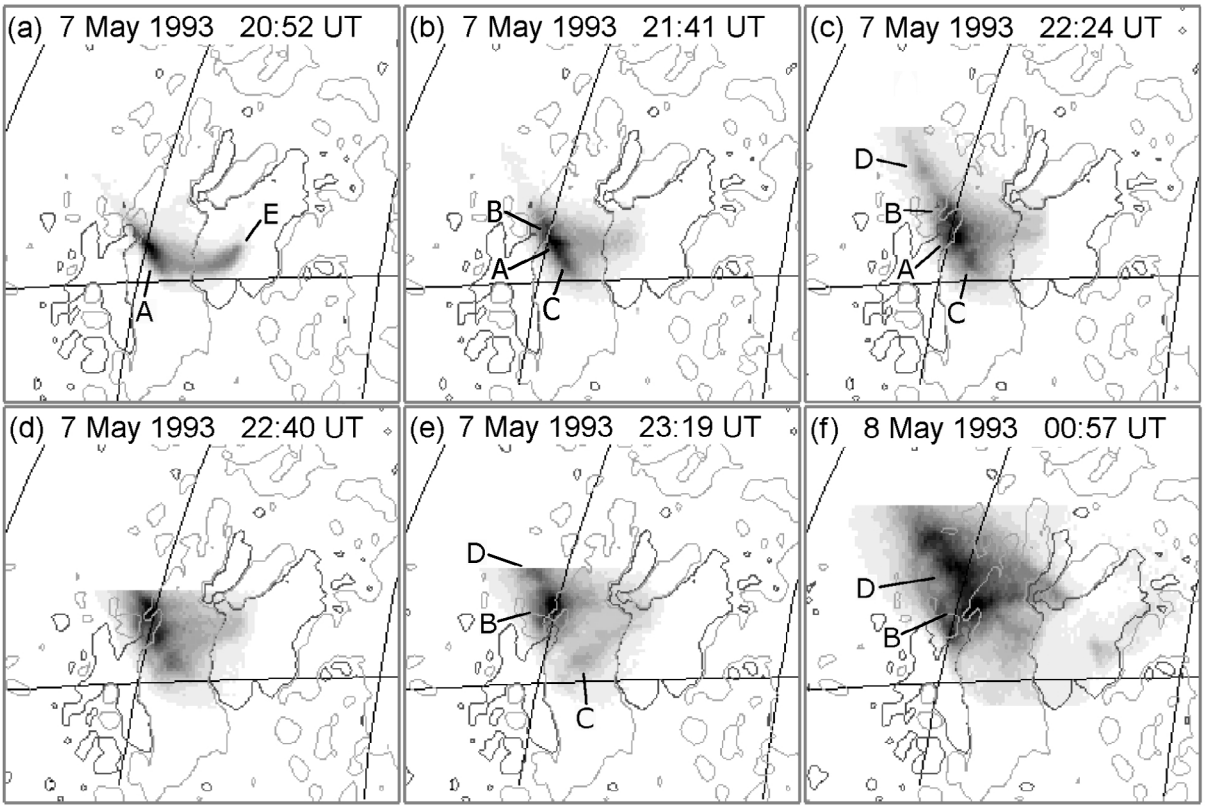

Fig. 2. Sequence of *Yohkoh*/SXT images in the Al12 filter for the 7 May 1993 flare. In each image the heliographical grid and magnetic field configuration taken from the KPVT magnetogram were overlaid (light-grey line: +5 Gs, dark-grey line: −5 Gs). The magnetogram was made on 7 May, before the beginning of the flare. The kernel D is not visible in images **d)** and **e)** because it is out of the image frame.

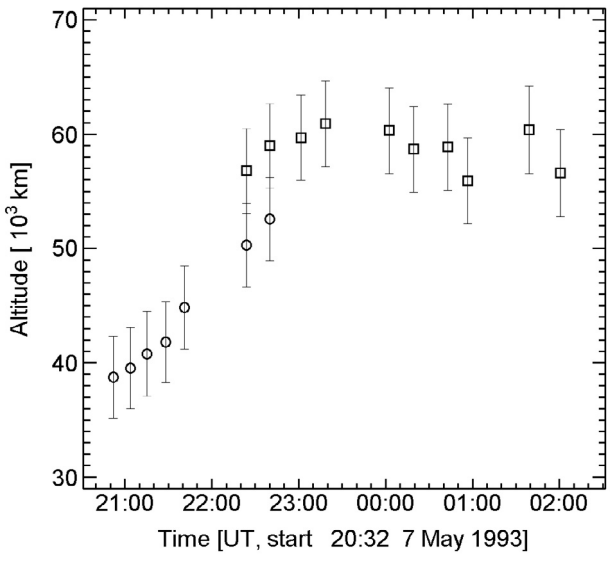

Fig. 3. Time-variations of the altitudes of the kernel A (circles) and the kernel B (squares) of the 7 May 1993 flare.

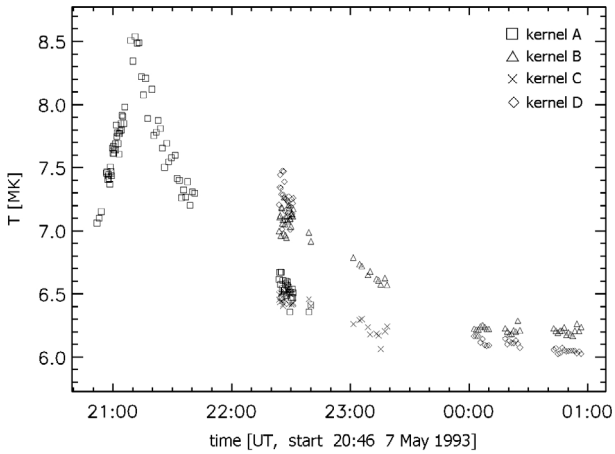

Fig. 4. Time-variations of temperature for the kernels of the 7 May 1993 flare. The temperature was obtained from Al12 diagnostics.

22:00 UT. Kernels A and C had almost the same T (about 6.5 MK) and kernels B and D were about 0.7 MK hotter. This suggests that there was some physical connection between the kernels A and C. The connection might be enabled by a magnetic tube (arcade channel) running along the tops of the loops. The same situation occurred in the case of the pair B–D. The connection between the two pairs was weaker. This conclusion is confirmed by the time-evolution. The kernels A and C disappeared much earlier than kernels B and D. The electron density of the analysed kernels is shown in Fig. 5. The maximum value of N was reached at 21:30 UT (8×10^{10} cm^{-3} for the kernel A). At 1:00 UT the density of the two remaining kernels, B and D, decreased to 1×10^{10} cm^{-3}.

The HXR flux coming from the analysed flare exceeded the sensitivity of HXT only during the flare maximum (see Fig. 6). Most of HXR emission occurred in channel L. Higher energies were reached only during the strongest pulses. The emission in channel L was dominated by a smooth component. Pulses were rather weak and meagre. In higher channels we can see only the impulsive component. Thus, the HXR curves of this flare

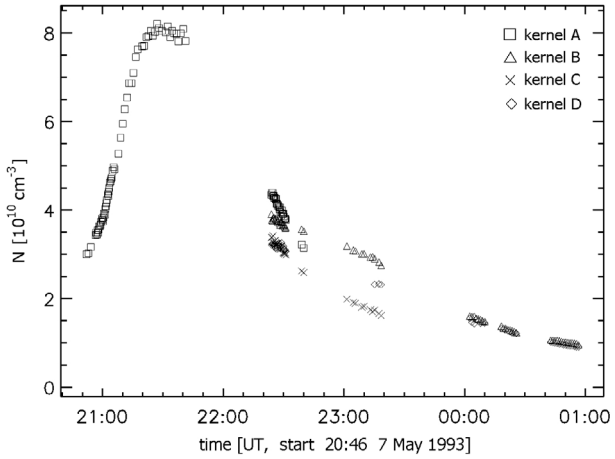

Fig. 5. Time-variations of density for the kernels of the 7 May 1993 flare. The density was obtained from Al12 diagnostics.

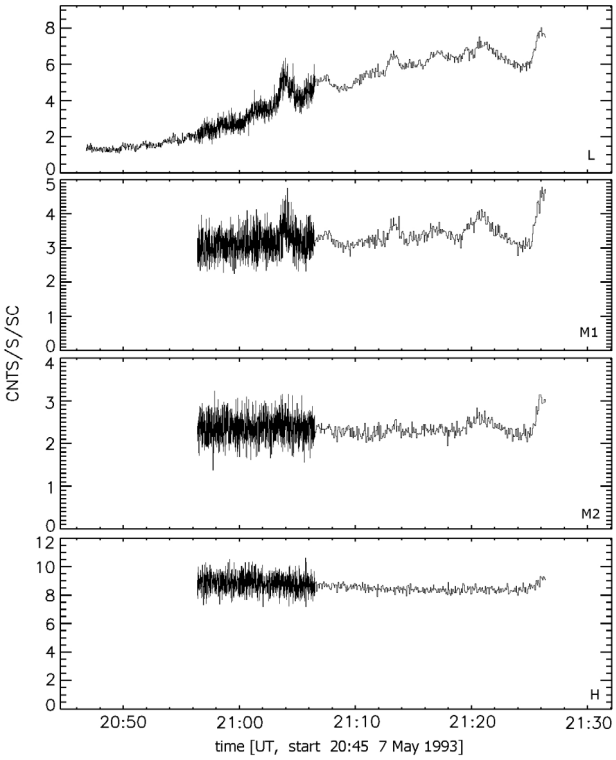

Fig. 6. HXR fluxes for the 7 May 1993 flare measured by *Yohkoh*/HXT in four channels.

resemble curves of flares with occulted footpoints (see Tomczak 2001). This suggests that HXR emission of the analysed flare came mainly from loop-top sources and footpoint sources were weak. This conclusion is confirmed by HXT images.

The hardness ratio R for smooth component did not exceed 0.05 (see Fig. 7). This indicate thermal emission of 20 MK plasma. The plasma was contained inside or close to the kernel A (see HXT images in Fig. 8). Pulses had R of about 0.4−0.9, thus this was non-thermal emission with spectral index $\gamma = 3.0-5.4$. This emission came mainly from the kernel A.

Only in channel L was the number of counts sufficient to obtain HXT images for the 7 May 1993 flare. Figure 8 shows a sequence of selected HXR images overlaid on SXT/Be119 images. In the most HXT images one can see only one bright source, which was located at almost the same position as the kernel A.

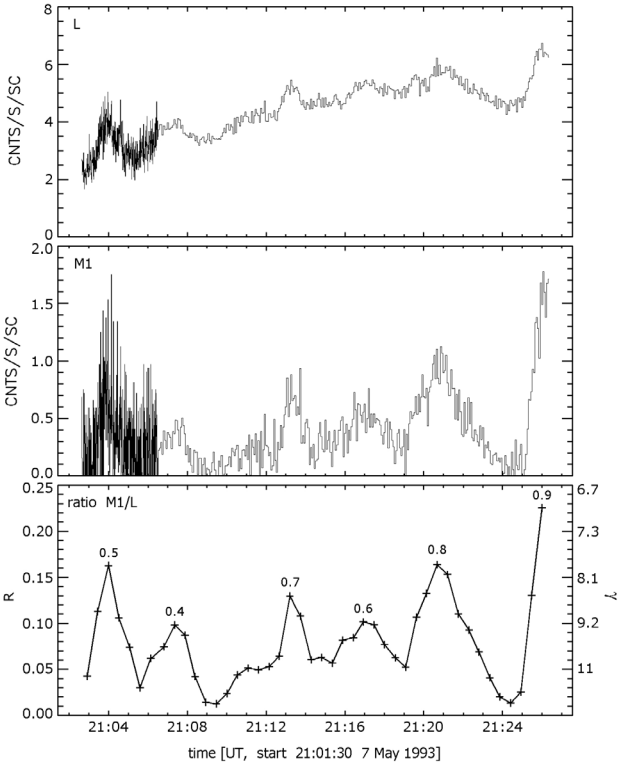

Fig. 7. HXR fluxes for the 7 May 1993 flare measured by *Yohkoh*/HXT in channels L and M1 (*two upper panels*; background is subtracted). Hardness ratio R and spectral index γ (*bottom panel*) estimated from measurements in these two channels. Numbers at the maxima indicate their R after subtraction of the smooth component.

Initially the centre of the source was situated in the centre of the kernel A. Later on it drifted along the major axis of the kernel, toward the north end and simultaneously became more elongated. It is worth to notice that the major axis of this source agreed with the major axis of the kernel A. Other HXR sources seen in Figs. 8a,d,f were probably related to the kernels B, C and D which appeared later in SXT images. HXR sources situated to the right of the kernel A (see Figs. 8b,e,f) were probably footpoints. Figures 8e,f are interesting. In these images we can see faint HXR structures, which connected elongated loop-top sources with footpoint sources. They looked like loops "legs" and the whole HXR structure resembled an arcade. The elongated shape of HXR loop-top source may indicate the presence of the arcade channel.

3.2. The 14 May 1993 flare

This flare occurred at N19 W48, in the same active region as the 7 May 1993 flare (AR 7500). It began at 21:55 UT and had two maxima. The first one (M1.4) was at 22:05 UT, then SXR flux decreased until 22:26 UT. The second, higher maximum (M4.4) was reached at 22:58 UT. After this, flare flux decreased for about 8 h. Figure 9 shows *GOES*/SEM X-ray fluxes versus time for the described flare. *Yohkoh*/SXT images show that both maxima occurred in the same structure.

Yohkoh observations cover the whole duration of the 14 May 1993 flare. Selected *Yohkoh*/SXT images of the flare are shown in Fig. 10. During the flare rise-phase and the first maximum, one elongated and low-altitude kernel (the kernel L) was seen in SXT images (see Fig. 10a). There were no *Yohkoh* observations between 22:25 and 23:05 UT due to the satellite

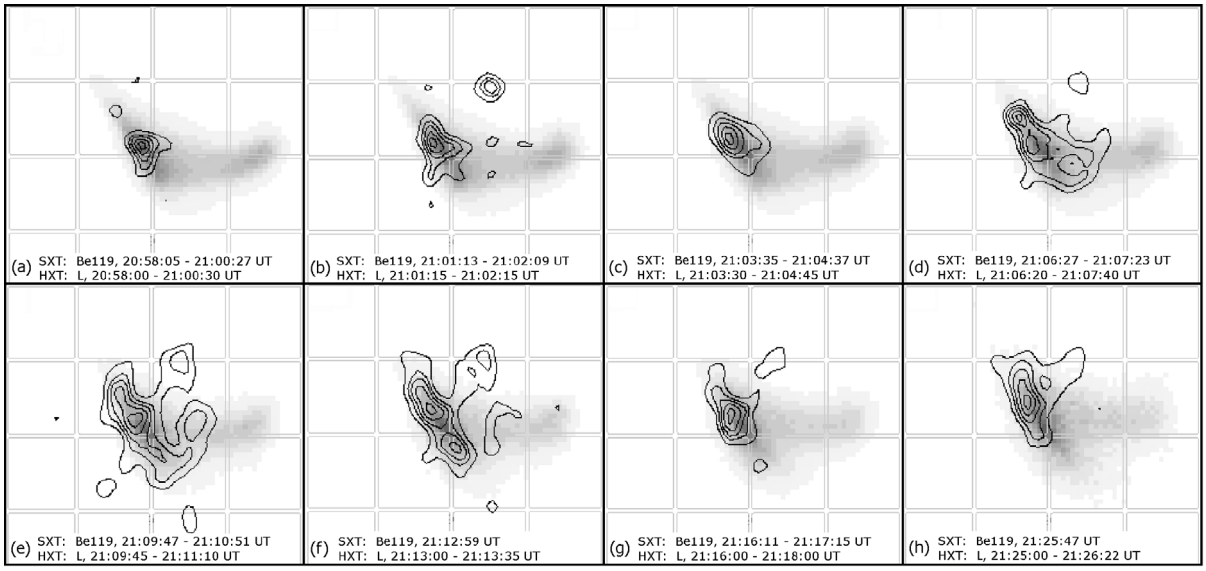

Fig. 8. Sequence of selected HXR images (contours) of the 7 May 1993 flare overlaid on SXT/Be119 images (in gray). The contours have the following values: 0.20, 0.35, 0.50, 0.70, 0.90 of the brightest pixel in each image. All images have size 64 × 64 SXT pixels.

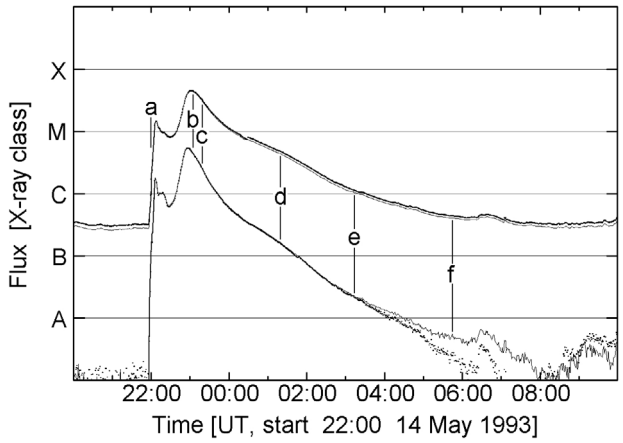

Fig. 9. *GOES*/SEM X-ray fluxes for the 14 May 1993 flare (upper curve: 1–8 Å, lower curve: 0.5–4 Å). Vertical lines indicate the observation time of the *Yohkoh*/SXT images shown in Fig. 10.

night. This situation is very inconvenient because after this satellite night we can see a high arcade with several loop-top kernels. The lack of observations makes it impossible to tell how the flare transformed from the low-altitude kernel L to this high arcade. In Fig. 10b, there are three kernels: A, B and C. Ten minutes later fourth kernel appeared in SXT images (see Fig. 10c). After the next satellite night, we see that the kernels B and C disappeared and in their position there was a bright "tube" which we called channel BC (see Fig. 10d). Between about 1:00 and 2:30 UT on 15 May, the kernel D was the biggest and brightest one. At the same time we can see two subkernels in the kernel (D1 and D2). Just after 3:00 UT the kernel D began to disappear from its southern end – first subkernel D1 then subkernel D2 (see Fig. 10e). After 4:00 UT the channel BC disappeared and there remained only one kernel – the kernel A (see Fig. 10f). This kernel disappeared 1.5 h later. In the case of this flare the arcade channel could be seen clearly in some SXT images (see Fig. 10e). The 14 May 1993 flare is similar to the 7 May 1993 flare. Both flares had one elongated kernel during the rise phase and a high arcade with several kernels during the decay phase.

The sequence of SXR images clearly shows the upward expansion of the arcade. We estimated the altitudes of the flare kernels. The results are shown in Fig. 11. The figure shows upward expansion of the arcade starting at about 21:50 UT with a velocity of about 10 km s^{-1}, and that was systematically decelerated to zero after 4 UT.

Yohkoh/SXT observations allow us to determine T, ϵ and N for the flare kernels. Because the kernels B and C were not well separated, they were analysed as one structure (the kernel B+C). Because the Be diagnostics is available only before 23:54 UT, we present results from the Al diagnostics, which covers the whole duration of the event. Figure 12 shows obtained values of the kernels temperature. The kernel L changed its T very fast – in ten minutes the temperature rose from 7.2 to 8.2 MK and dropped back to 7.1 MK. The time-scale of this changes was much shorter than for the kernels A, B, C and D. This may suggest that the kernel L was not a precursor of any of these kernels. The maximal observed temperature of the decay-phase kernels was about 7.5–8.0 MK. The most interesting are the time-intervals of constant T. Such a situation occurred for example for the kernel A between about 3 and 4 UT. Its temperature stopped at 6.1 MK for more than 1 h (assuming no rapid variation during the satellite night). Such a behavior may provide interesting information about the energy release (see Paper II). Electron densities of the 15 May 1993 flare kernels are shown in Fig. 13. The maximal value of N (2×10^{11} cm^{-3}) was reached at 22:08 UT by the kernel L. The maximum of density for the kernels A, B+C and D was not observed due to the satellite night. Density during the decay phase dropped from 1×10^{11} cm^{-3} (the kernels A and B+C) and 6×10^{10} cm^{-3} (the kernel D) at 23:10 UT. After 6 UT the density of the last kernel (the kernel A) was only 6×10^{9} cm^{-3}.

The HXR flux of the 14 May 1993 flare was very high during the first maximum (see Fig. 14). Emission in all channels was dominated by a strong impulsive component. Two highest maxima can be seen, even in channel H. During and after the second maximum, emission in the channels L and M1 was dominated by a smooth component (see Fig. 15). The impulsive component was very weak – there were only two pulses in channel L; the first one also can be seen in the channels M1 and M2. No

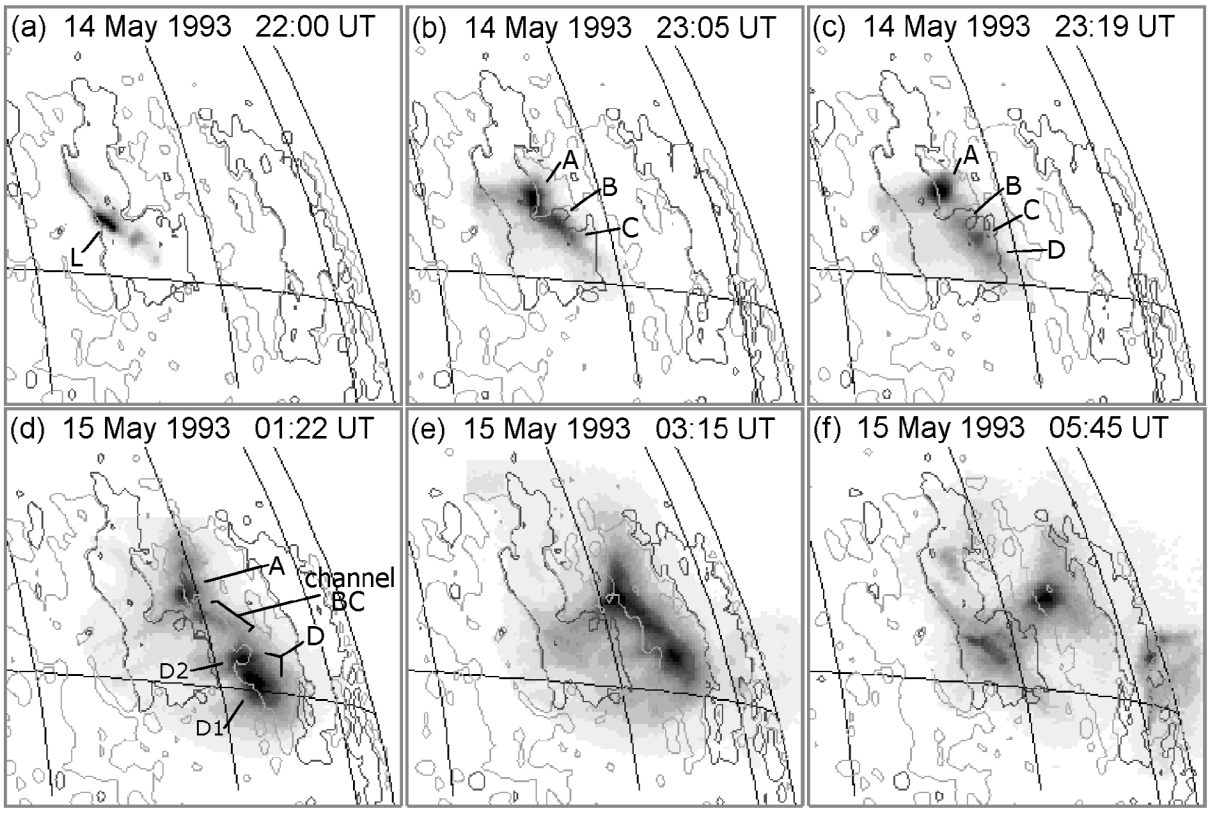

Fig. 10. Sequence of *Yohkoh*/SXT images in the Al12 filter for the 14 May 1993 flare. In each image the heliographical grid and magnetic field configuration taken from the KPVT magnetogram were overlaid (light-grey line: +5 Gs, dark-grey line: −5 Gs). The magnetogram was made about 8 h before the beginning of the flare.

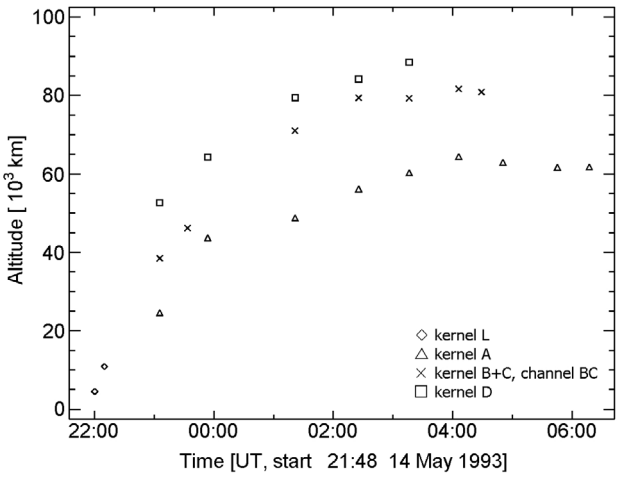

Fig. 11. Time-variations of the altitudes of the 14 May 1993 flare kernels. For clarity the error bars were omitted.

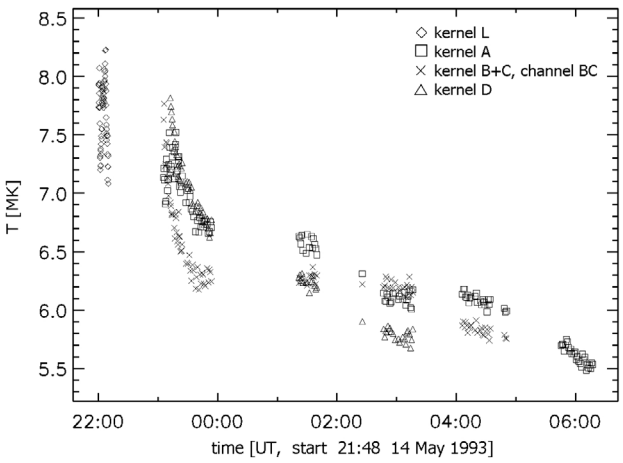

Fig. 12. Time-variations of temperature T for the kernels of the 14 May 1993 flare. The temperature was obtained from Al12 diagnostics.

emission was measured in channel H. The emission during the second maximum was similar to the HXR emission of the 7 May 1993 flare. Thus, we can conclude (and this is confirmed by HXT images) that the emission came mainly from loop-top sources.

During the first maximum, the hardness ratio for the smooth component was about 0.2−0.35 and for the impulsive component: 0.6−0.9 (see Fig. 16). Thus, the pulses were non-thermal emission with $\gamma = 3.0-4.2$. After the satellite night the R of the smooth component was 0.1−0.2 (see Fig. 17) which implies thermal emission of about 30 MK hot plasma. The plasma was placed just above the kernel A (see HXT images). The first of the two pulses that occurred at that time had the hardness ratio of about 0.6. This means that the emission was non-thermal ($\gamma \approx 4$). HXT images show that the pulse came from a footpoint source.

The quite high HXR flux of the 14 May 1993 flare allowed us to obtain images in channels L, M1 and M2. A sequence of selected HXT images overlaid on SXT/Be119 images is shown in Fig. 18. One bright source dominates in most HXT images made for the first maximum (see Figs. 18a–e). The centre of the source was situated at the centre of the kernel L and its size was almost

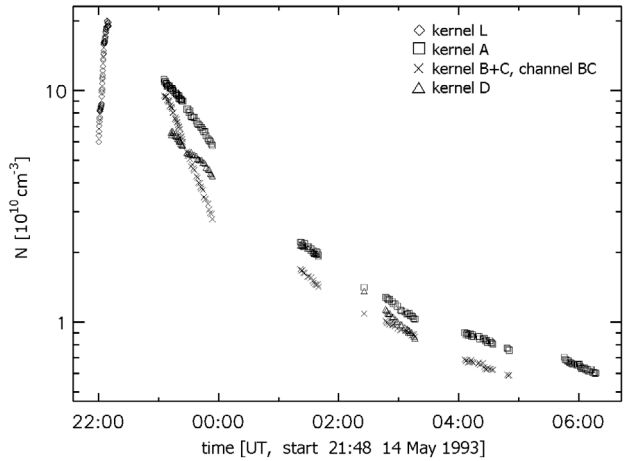

Fig. 13. Time-variations of density N for the kernels of the 14 May 1993 flare. The density was obtained from Al12 diagnostics.

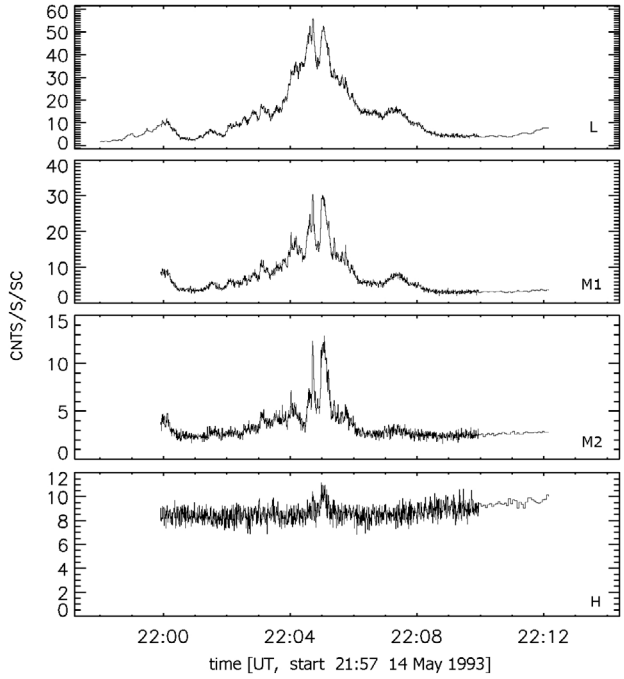

Fig. 14. HXR fluxes for the 14 May 1993 flare measured by *Yohkoh*/HXT in four channels during the first flare maximum.

the same as the kernel. Moreover, the source was sometimes elongated along the major axis almost parallel to the kernel L major axis (e.g. Fig. 18a). The other HXR sources, seen for example in Figs. 18c,d, were footpoint sources. This is confirmed by impulsive soft X-ray brightenings detected for the sources (Mrozek & Tomczak 2004; Mrozek – private communication). During the second maximum, the strongest source seen in channel L was located above the kernel A (see Figs. 18f,h). With time the source became more compact. In the channels M1 and M2 the number of counts was sufficient to obtain images only for the pulse seen on light curves at about 23:03 UT. The obtained images show that the emission of the pulse came most likely from a footpoint lying below the kernel D (see Fig. 18g).

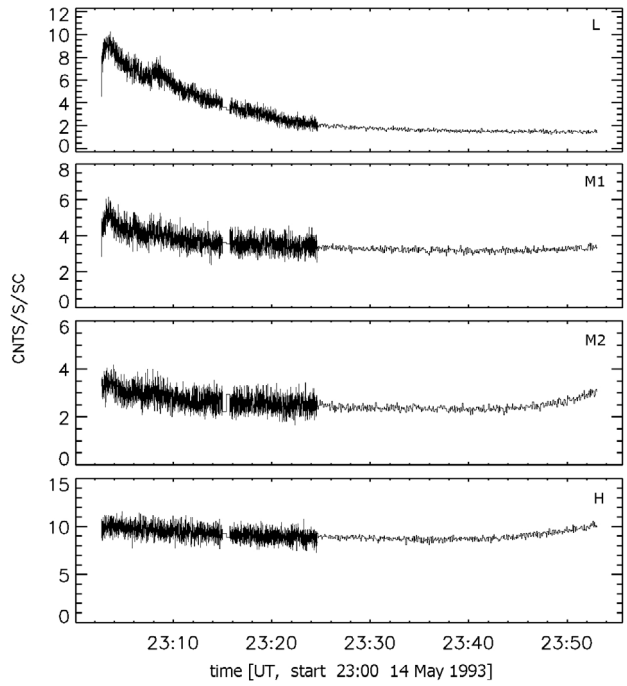

Fig. 15. HXR fluxes for the 14 May 1993 flare measured by *Yohkoh*/HXT in four channels during the second flare maximum.

3.3. The 27 April 1998 flare

The X1.0 flare of 27 April 1998 occurred in NOAA AR 8210 at S16 E50. The flare began at 8:36 UT (Hα observations) and was preceded by the slow increase of the soft X-ray (see Fig. 19). After the flare maximum, which was at 9:20 UT, the SXR flux very slowly decreased for about 20 h.

This flare was observed by *Yohkoh* from the beginning until 4 UT on 28 April. Figure 20 shows a sequence of *Yohkoh*/SXT images of the 27 April 1998 flare. At the flare beginning, several short, bright loops were seen in the central part of AR 8210 (see Fig. 20a). After the satellite night, a high arcade with two loop-top flare kernels (A and B) were seen in the northern part of the active region (see Figs. 20b–d). This flare very clearly showed bright structure (arcade channel) running along the tops of the flaring loops (e.g. Figs. 20b,c). In the late decay-phase of the flare (after 15:00 UT), kernels A and B became less clearly visible and the arcade channel was rather uniformly bright (see the Figs. 20e,f).

We can see that flare kernels A and B occurred at the crossings of the arcade channel and arcade loops. This phenomenon is particularly well illustrated by the kernel A. From about 13 UT to 14:30 UT in the kernel A two subkernels (A1 and A2) were visible. At the same time the loop connecting kernel A with the chromosphere split in two parts (see Fig. 20d). Subkernels A1 and A2 occurred exactly at the crossings of the arcade channel and split loop.

Upward expansion of the flare arcade is clearly visible in the *Yohkoh*/SXT images. Heights of the arcade were estimated by measuring the altitudes of the kernel A (which was brighter than the kernel B). We assumed that the altitude of the kernel B was the same as the altitude of the kernel A, because all arcade loops had similar lengths (see Fig. 20). The results are shown in Fig. 21. Upward expansion of the arcade started before 9:00 UT with a velocity of more than 2 km s^{-1} and was systematically decelerated. At about 4 UT on 28 April the velocity of the

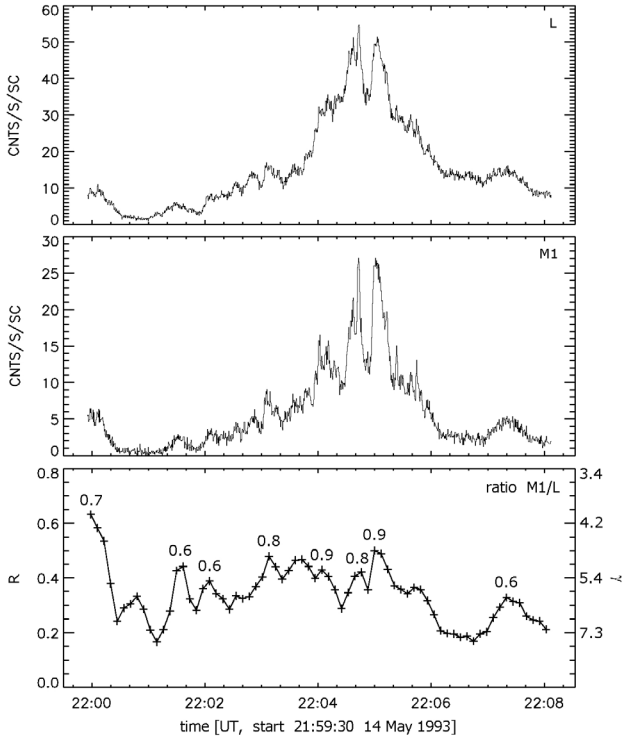

Fig. 16. HXR fluxes for the 14 May 1993 flare measured by *Yohkoh*/HXT in channels L and M1 during the first flare maximum (*two upper panels*; background is subtracted). Hardness ratio R and spectral index γ (*bottom panel*) estimated from measurements in these two channels. Numbers at the maxima indicate their R after subtraction of the smooth component.

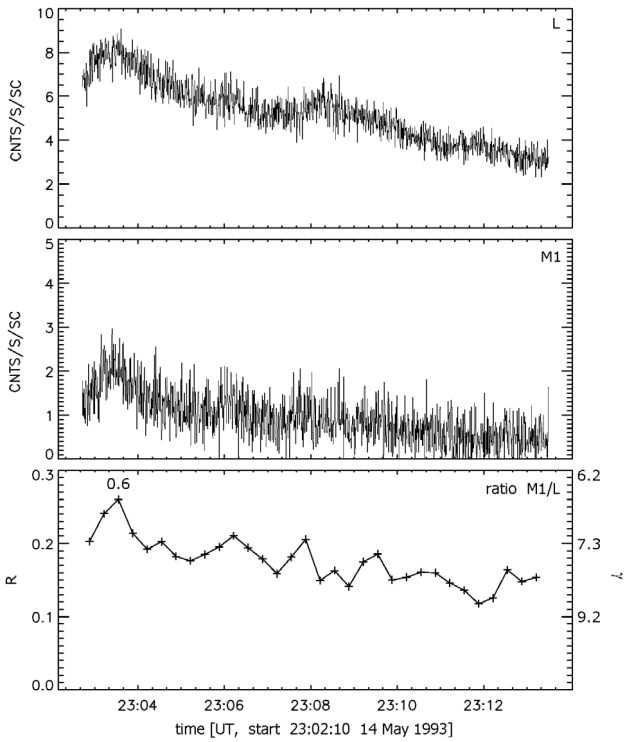

Fig. 17. HXR fluxes for the 14 May 1993 flare measured by *Yohkoh*/HXT in channels L and M1 during the second flare maximum (*two upper panels*; background is subtracted). Hardness ratio R and spectral index γ (*bottom panel*) estimated from measurements in these two channels. Numbers at the maxima indicate their R after subtraction of the smooth component.

expansion dropped below 1 km s^{-1} and the loop-top kernels reached an altitude of almost 9×10^4 km.

Using SXT images we derived T, ϵ and N for both of the flare kernels. Contrary to the May 1993 flares, both diagnostics (Be and Al) cover almost the whole duration of the flare. The exception is one satellite day during the late decay-phase for which only Al.1 images are available. However, we present only the Al diagnostics results to enable a comparison with the results for the May 1993 flares. As described above, after 15 UT the kernels A and B cannot be distinguished in the arcade channel. Thus, from this moment to the end of the flare we analyze the channel as one structure with no substructures. Temperatures obtained for the kernels and the channel are shown in Fig. 22. The maximum of T was not observed due to the satellite night. The highest observed temperature of the kernels was about 7.6 MK. Both kernels had almost the same temperature during their evolution. At the end of the flare, T of the channel dropped below 6.0 MK. Figure 23 shows density versus time for both kernels and for the whole channel after the kernels disappeared. As in the case of temperature, the maximum of N was not observed. During the whole decay phase of the flare, the density monotonically decreased from about 1×10^{11} cm^{-3} to 5×10^9 cm^{-3}. As we can see the brighter kernel A had almost the same or higher density than the kernel B.

The HXR emitted by the analysed flare was high enough to be detected by HXT from 8:50 UT to 10:05 UT. Before the beginning of the satellite night (8:56 UT) HXR emission came from several short, bright loops seen in SXT images. Because a relation between these loops and the high arcade is unclear, we decided to analyse only HXR measured after the satellite night (from 9:36 UT) and coming beyond a doubt from the arcade. At that time HXR emission was weak (see Fig. 24). The emission in channel L was dominated by a smooth component. There was only one, rather smooth and wide pulse. In the higher channels M1 and M2 only two pulses could be seen: the first is the same as in channel L and the second, very weak, occurred at 9:44 UT. No signal was measured in channel H.

The hardness ratio R for the smooth component was about 0.05–0.10 (see Fig. 25). Thus, the component was emitted by 20–30 MK hot plasma. The plasma was placed mainly just above the kernel A (see HXT images in Fig. 26). The stronger of the two recorded pulses had $R = 0.4$. This suggests non-thermal emission with a spectral index $\gamma = 5.5$. The emission might come from the loop footpoint below the kernel A.

The HXR flux coming from the analysed flare was sufficient to obtain HXR images only in channel L and M1. Results are shown in Fig. 26, where selected HXT images are overlaid on SXT/Be119 images. The HXR emission in channel L was dominated by high-altitude sources. The first obtained HXT image (see Fig. 26a) shows a broad, elongated HXR structure running along and above the SXT arcade. The brightest part of the structure was situated above the kernel A. During next three minutes the structure became more compact (see Fig. 26b) and we see only the elliptical source (A_{HXT}) just above the kernel A. In some HXT images one can see also the weak source (B_{HXT}) above the kernel B (see Fig. 26c). For channel M1 we obtained only one image (see Fig. 26d). The image shows that emission of the strongest recorded pulse came from a footpoint source below the kernel A.

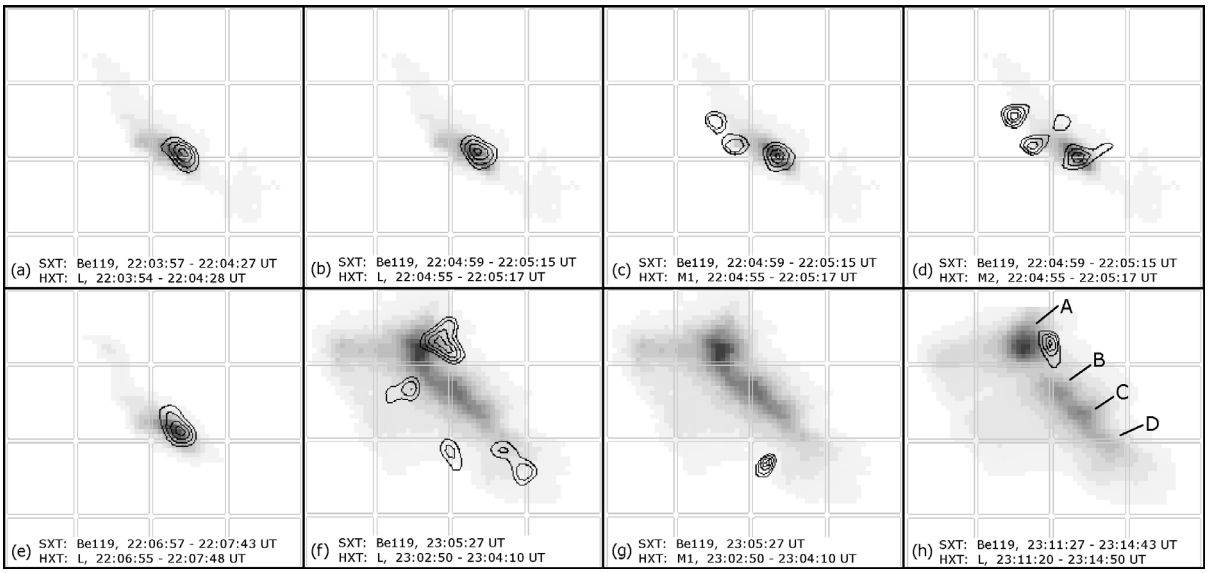

Fig. 18. Sequence of selected HXR images (contours) of the 14 May 1993 flare overlaid on SXT/Be119 images (in gray). The contours have the following values: 0.20, 0.35, 0.50, 0.70, 0.90 of the brightest pixel in each image. All images have size 64 × 64 SXT pixels.

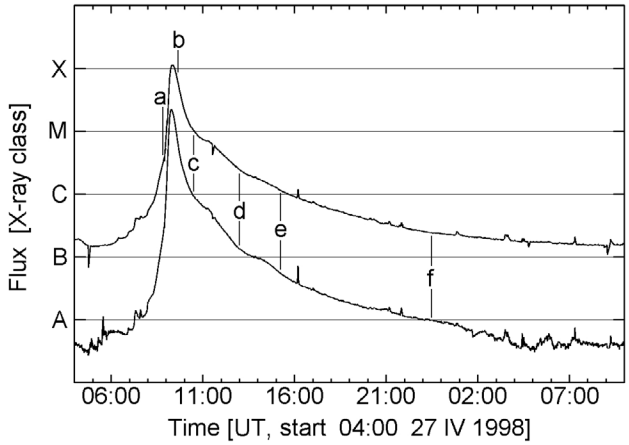

Fig. 19. *GOES*/SEM X-ray fluxes for the 27 April 1998 flare (upper curve: 1–8 Å, lower curve: 0.5–4 Å). Vertical lines indicate the observation time of the *Yohkoh*/SXT images shown in Fig. 20.

4. Discussion

4.1. Morphology

1. In the paper of Jakimiec et al. (1997) and Tomczak (1994) the authors suggested that a so-called arcade channel – a magnetic tube running along the tops of arcade loops – may be present in arcade flares. In our study we found some observational evidence for the existence of such a channel: (1) In some SXT images we can see a bright structure running along the tops of the loops (e.g. Figs. 10d,e and 20b–d; areas between the loop-top kernels are fainter than the kernels but brighter than the rest of the surroundings). (2) In HXT images we found elongated structures located at the tops of the loops (see Figs. 8e,f and 26b).
   The so-called dark filament and its eruption is a common observational structure of the initial stages of arcade-flares evolution. Also in theoretical models of arcade flares a magnetic tube (dark filament) perpendicular to arcade loops is present (e.g. Hirose et al. 2001; Uchida et al. 1999) and plays an important role in accumulating and releasing the magnetic energy. We can expect some relation between the dark filament and arcade channel. Further observational and theoretical study is needed to clarify this relation.
   The presence of an arcade channel would have two interesting consequences. Firstly, loop-top kernels would be located at crossings of the arcade channel and arcade loops. This phenomenon is particularly well illustrated when two subkernels are seen in a kernel (e.g. the kernel A of the 27 April 1998 flare). At the same time a loop connecting this kernel with the photosphere is split in two parts. Secondly, it was shown by Jakimiec et al. (1997) and Jakimiec (2002b) that a configuration with perpendicular magnetic tubes may leads to development of MHD turbulence. The SXT spectra of all flares (even during the decay phase) show a significant non-thermal line broadening (NTLB; Antonucci et al. 1982; Fludra et al. 1989). This NTLB is larger than if due to thermal motion. It is thought that at least a part of the observed NTLB is due to turbulent plasma motion in kernels. Since *Skylab* observations, it has been suggested that some restrictions to a flow of mass and energy out of the kernels to loops "legs" must exist. The MHD turbulence can provide such restriction (see Jakimiec et al. 1998).
2. Individual LDAFs kernels may occur in SXT images at different moments of the flare evolution. Some kernels occurred at the beginning of a flare (the kernel A of the 7 May 1993 flare), others just after the flare maximum (the kernel D of the mentioned flare). The duration of the kernels is also different, e.g. the kernel A of the 14 May 1993 flare existed for about 8 h while the kernel C of the 7 May 1993 flare only 2 h. These differences may indicate that the situation leading to formation of a flare kernel can occur not only at the beginning of a flare but also after the flare maximum. The duration of an individual kernel is determined by three factors: (1) duration of the magnetic field configuration maintaining the reconnection process; (2) amount of energy contained in the magnetic field and (3) the rate of energy dissipation.
   Moreover, the evolution of LDAFs, determined by the magnetic field configuration in a flare area, may be different. In some cases all kernels appear and disappear almost simultaneously (see the 27 April 1998 flare). The kernels may also

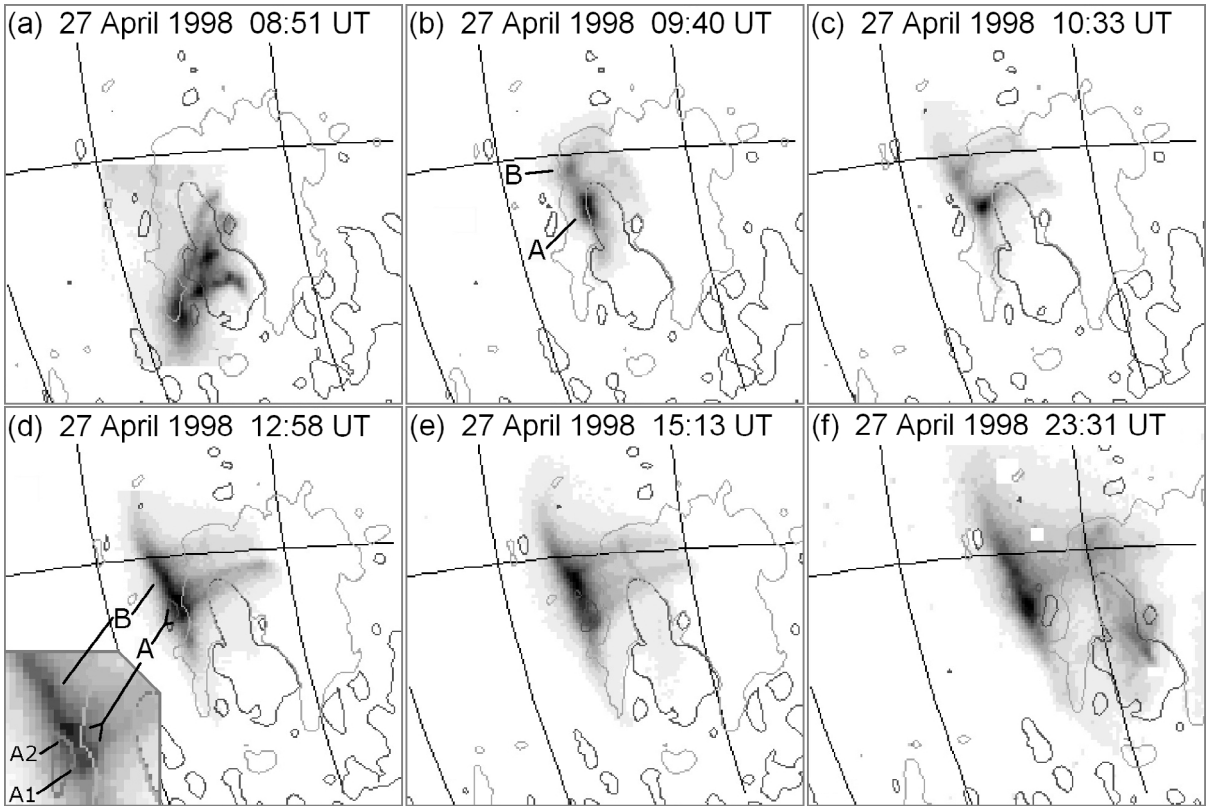

Fig. 20. Sequence of *Yohkoh*/SXT images in the Al12 filter for the 27 April 1998 flare. In each image the heliographical grid and magnetic field configuration taken from the Kitt Peak magnetogram were overlaid (light-grey line: +5 Gs, dark-grey line: −5 Gs). The magnetogram was made on 27 April 1998 during the decay phase of the flare. The inset in the bottom corner of the image **d)** shows a magnification of the flare kernels.

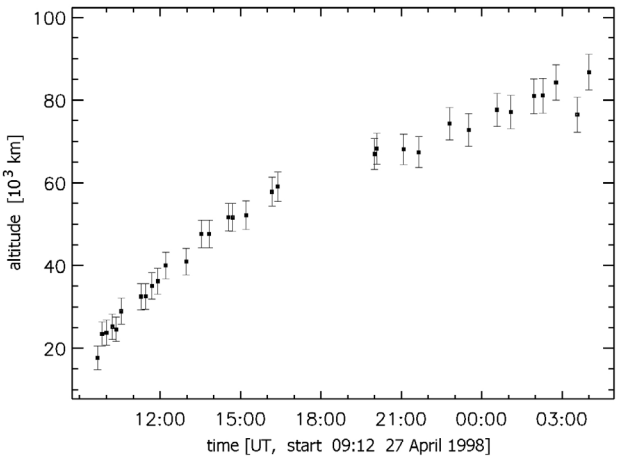

Fig. 21. Time-variations of the altitudes of the 27 April 1998 flare kernels.

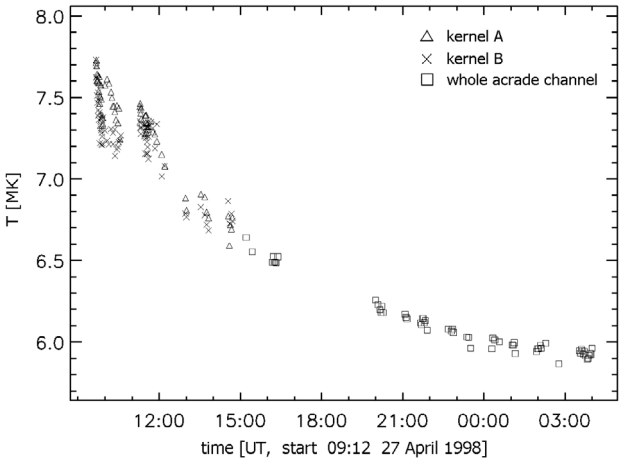

Fig. 22. Time-variations of temperature T for the kernels of the 27 April 1998 flare. The temperature was obtained from Al12 diagnostics.

appear and disappear one after the other as in both flares of May 1993 (e.g. the first kernel of the 7 May flare (the kernel A) disappeared just after formation of the kernels B, C, D; the kernel D of the 14 May flare appeared last and disappeared first).

The presence of several loop-top kernels in one LADF suggests that energy release in these flares occurs in several places simultaneously (see also Tomczak 1997 and Paper II). Differences in the moments of kernel appearance and disappearance, in time of their duration and in values of the physical parameters may provide information about the reconnection process in LDAFs. It means among other things that the reconnection process is not uniform along the flaring arcade. Moreover the process can develop either progressively along the arcade (e.g. the 14 May 1993 flare) or nearly simultaneously (e.g. the 27 April 1998 flare).

3. LDAFs kernels are large structures. Their radius is about $(1.0–1.5) \times 10^4$ km. The height of LDAFs arcade loops grows during the flare evolution with their velocity decreasing from several km s^{-1} at the flare beginning to less than 1 km s^{-1} in the late decay-phase. At the end of a flare the height may sometimes reach almost 10^5 km. This confirms

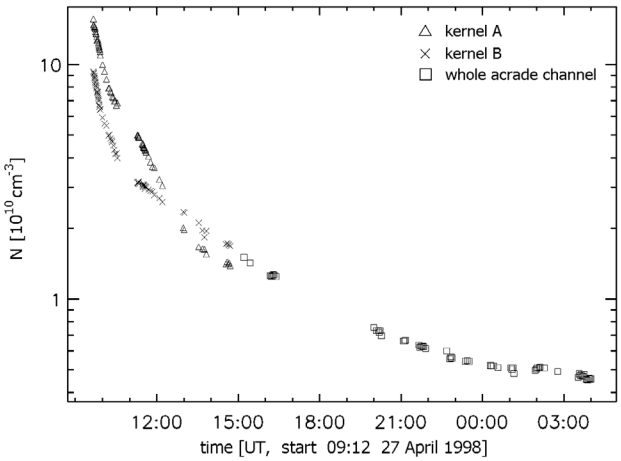

Fig. 23. Time-variations of density N for the kernels of the 27 April 1998 flare. The density was obtained from Al12 diagnostics.

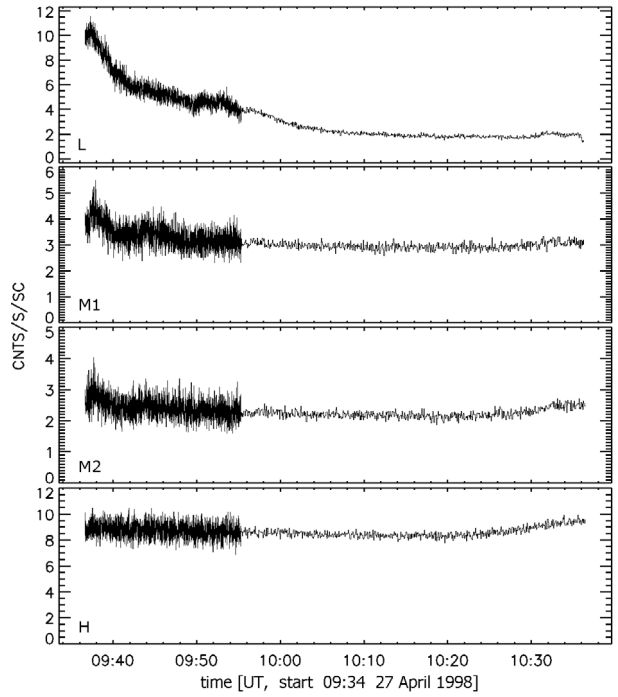

Fig. 24. HXR fluxes for the 27 April 1998 flare measured by *Yohkoh*/HXT in four channels.

results obtained by other authors from *Skylab* data (e.g. Kahler et al. 1977).

4. During the rise phase of both May 1993 flares, HXT images were dominated by one compact source. The source was situated close to the SXR kernel. Distance between centroids of the source and the kernel was always smaller than about 5×10^3 km (comparable with the kernel size). Besides this main source there were also HXR footpoint sources. Such a situation was not observed for the 27 April flare but this may be caused by the satellite night. After the maximum of the 14 May and 27 April flares, when arcades of loops were visible in SXT images, the main HXT/L sources were situated about 10^4 km above the main kernels. In HXT/M1(M2) images of these two flares only footpoint sources were seen. The HXR sources above SXR kernels contained hot plasma at temperature of 20−30 MK. The cooling times due to conductive losses for these sources are of the order of 10−100 s, 10 to 100 times shorter than the duration of the HXR sources. Thus, there had to be some continuous energy release during the decay phase to balance the losses and to support the sources existence. Therefore, the presence of the hot HXR sources is indirect evidence of energy release in LDAFs after their maximum. Such sources were not observed for the 7 May flare, possibly due to the satellite night, which started just after the flare maximum.

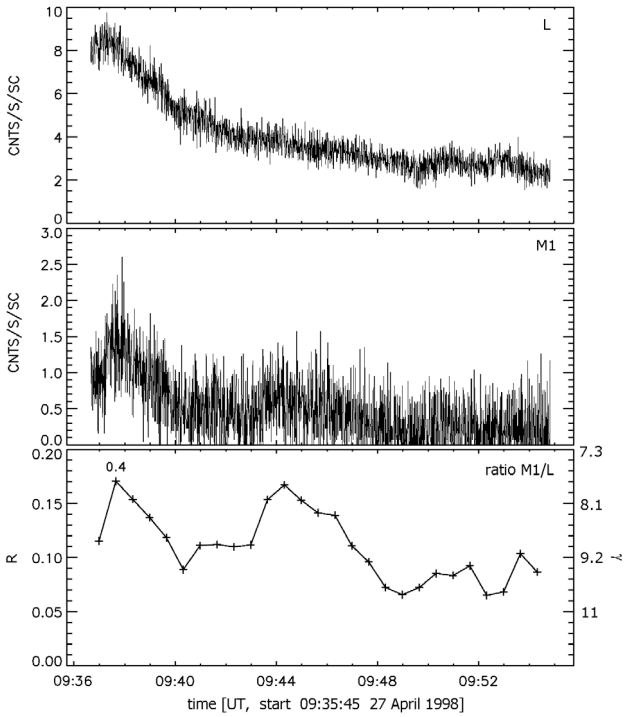

Fig. 25. HXR fluxes for the 27 April 1998 flare measured by *Yohkoh*/HXT in channels L and M1 (*two upper panels*; background is subtracted). Hardness ratio R and spectral index γ (*bottom panel*) estimated from measurements in these two channels. Numbers at the maxima indicate their R after subtraction of the smooth component.

4.2. Physical parameters

1. LDAFs kernels are not very hot. The maximum "mean" temperature of the analysed kernels was about 10 MK (value taken from the Be diagnostics). However just above the kernels there was also very hot plasma (20−30 MK) seen in HXT images even after the flares maxima.
2. The maximum density of the kernels was of the order of 10^{11} cm^{-3}. This is a typical value of N for different types of solar flares.

The comparison of the parameters obtained from the Be119 and Al12 diagnostics leads to the following conclusions:

1. Temperature T_B is always greater than temperature T_A. Difference between T_B and T_A is significant and grows with temperature of a kernel. In the case of the analysed kernels the value of $(T_B - T_A)$ was in the range of 1−2.5 MK.
2. The emission measure ϵ_B and density N_B are always smaller than ϵ_A and N_A. However, values of $(\epsilon_A - \epsilon_B)$ and $(N_A - N_B)$ are small and comparable with the errors of ϵ and N, respectively.

Significant and systematic differences between T_B and T_A, growing with the temperature of a kernel, can be the result of its

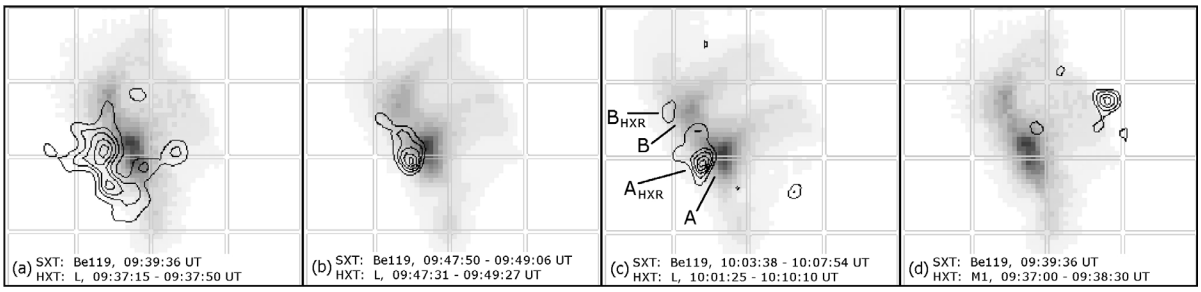

Fig. 26. Sequence of selected HXR images (contours) of the 27 April 1998 flare overlaid on SXT/Be119 images (in gray). The contours have the following values: 0.20, 0.35, 0.50, 0.70, 0.90 of the brightest pixel in each image. All images have size 64×64 SXT pixels.

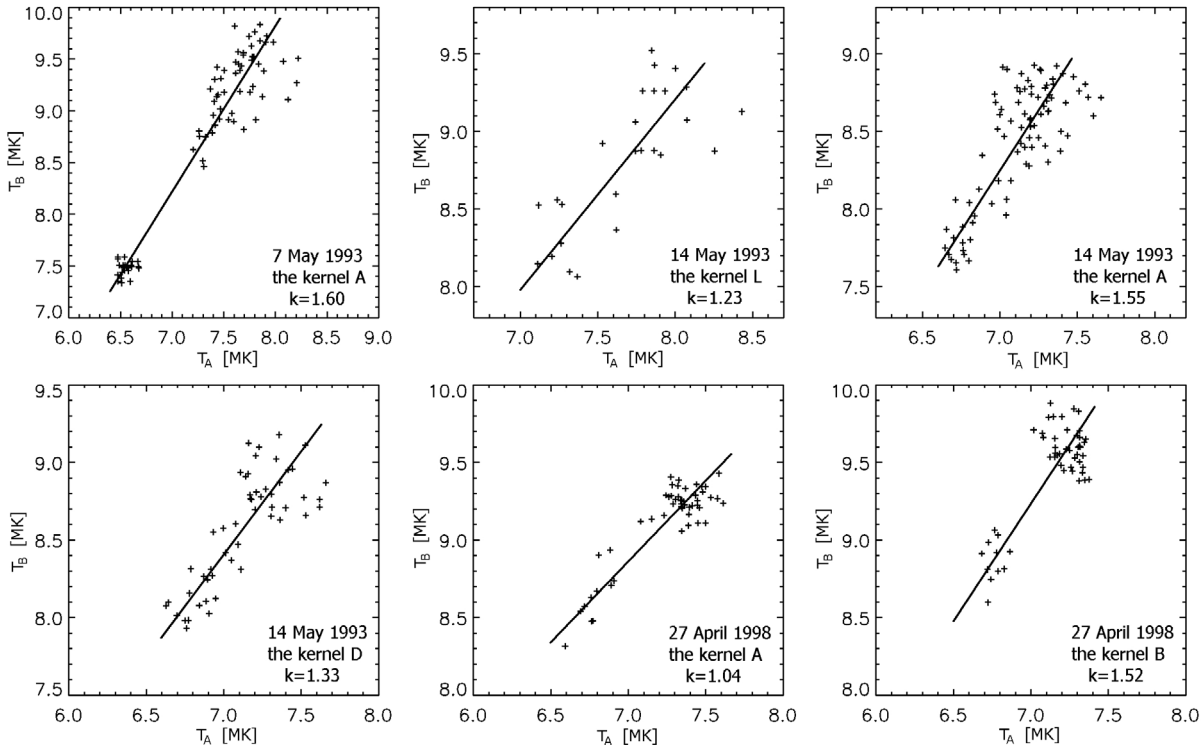

Fig. 27. Relationship between T_B and T_A for some of the analysed kernels. Straight lines were fitted using the least square method. Values of obtained slopes k are given in each graph. See text for details.

multithermal nature. In a such case T_B will be greater than T_A because the Be119 diagnostics is more sensitive to hotter plasma than the Al12 diagnostics. In order to be sure that this is not an instrumental effect, we have displayed graphs of T_B vs. T_A (see Fig. 27). For each kernel we fitted a straight line using the least-square method. Obtained values of slopes k are given in Fig. 27. If differences between T_B and T_A were caused only by instrumental effects, the slope k would be the same for all kernels or there would be some difference between k for the kernels of the two 1993 flares and k for the kernels of the 1998 flare caused by aging of *Yohkoh*. However, the slopes k differ not only for the kernels of different flares, but also for kernels of the same flare. Thus, we can conclude that the analysed kernels were multithermal and different values of k indicate that there were different relative contents of hotter and cooler plasma and different time-evolution of these contents.

5. Conclusions

LDAFs have a more complicated structure than compact flares, however their investigation can help us in better understanding processes that occur in flaring structures. In this paper we investigate the morphology and physical parameters of these flares. The conclusions of our investigation are as follows:

1. Observations suggest that a magnetic tube (so-called arcade channel) perpendicular to arcade loops may exist in LDAFs. It was shown by Jakimiec (2002b) that such an interaction between the arcade channel and arcade loops may lead to development of MHD turbulence in loop-top kernels. The turbulence can reduce the flow of mass and energy out of the kernels to loops "legs" (see Jakimiec et al. 1998). Such reduction has been suggested by other authors using *Skylab* observations.
2. The energy release in LDAFs occurs in several places simultaneously. The reconnection process is not uniform along the flaring arcade.
3. The analysis of HXT observations showed that even during the decay phase hot plasma (20−30 MK) is present in LDAFs. This is indirect evidence of energy release in LDAFs after their maximum.

The X-Ray Telescope (XRT) and EUV Imaging Spectrograph (EIS) onboard the new solar observatory *Hinode* will provide observations with better quality than *Yohkoh*. The observations will allow us to continue the study of processes taking place in LDAFs.

Acknowledgements. I thank the *Yohkoh*, KPVT and *GOES*/SEM teams for the excellent observations and Prof. J. Jakimiec and Prof. M. Tomczak for discussions and reviewing of this manuscript.

References

Acton, L. W., Feldman, U., Bruner, M. E., et al. 1992, PASJ, 44, L71
Antonucci, E., Gabriel, A. H., Acton, L. W., et al. 1982, Sol. Phys., 78, 107
Choe, G. S., & Lee, L. C. 1996a, ApJ, 472, 360
Choe, G. S., & Lee, L. C. 1996b, ApJ, 472, 372
Donnelly, R. F., Grubb, R. N., & Cowley, F. C. 1977, NOAA Tech. Memo. ERL SEL-48
Doschek, G. A., Strong, K. T., & Tsuneta, S. 1995, ApJ, 440, 370
Feldman, U., Seely, J. F., Doschek, G. A., & Brown, C. M. 1995, ApJ, 446, 860
Fludra, A., Bentley, R. D., Lemen, J. R., Jakimiec, J., & Sylwester, J. 1989, ApJ, 344, 991
Frieden, B. R. 1972, J. Opt. Soc. Am., 62, 511
Gerassimenko, M., & Nolte, J. T. 1978, Sol. Phys., 60, 299
Gull, S. F., & Daniell, G. J. 1978, Nature, 272, 686
Hara, H. 1992, Master thesis, Dept. of Astronomy, University of Tokyo
Hara, H., Tsuneta, S., Lemen, J. R., Acton, L. W., & McTiernan, J. M. 1992, PASJ, 44, L135
Harra-Murnion, L. K., Schmieder, B., van Driel-Gesztelyi, L., et al. 1998, A&A, 337, 911
Hirose, S., Uchida, Y., Uemura, S., Yamaguchi, T., & Cable, S. B. 2001, ApJ, 551, 586
Isobe, H., Yokoyama, T., Shimojo, M., et al. 2002, ApJ, 566, 528
Jakimiec, J. 2002a, Adv. Space Res., 30, 577
Jakimiec, J. 2002b, Adv. Space Res., 29, 1101
Jakimiec, J., Tomczak, M., Fludra, A., & Falewicz, R. 1997, Adv. Space Res., 20, 2341
Jakimiec, J., Tomczak, M., Falewicz, R., Phillips, K. J. H., & Fludra, A. 1998, A&A, 334, 1112
Kahler, S. 1977, ApJ, 214, 891
Kopp, R. A., & Pneuman, G. W. 1976, Sol. Phys., 50, 85
Kosugi, T., Masuda, S., Makishima, K., et al. 1991, Sol. Phys., 136, 17
Livingston, W. C., Harvey, J., Pierce, A. K., et al. 1976, Appl. Opt., 15, 33
Morita, S., Uchida, Y., Hirose, S., Uemura, S., & Yamaguchi, T. 2001, Sol. Phys., 200, 137
Mrozek, T., & Tomczak, M. 2004, A&A, 415, 377
Sakao, T. 1994, Ph.D. Thesis, Dept. of Astronomy, University of Tokyo
Sato, J. 1997, Ph.D. Thesis, Graduate Univ. of Advanced Studies, Tokyo
Sato, J., Kosugi, T., & Makishima, K. 1999, PASJ, 51, 127
Sheeley, N. R., Bohlin, J. D., Brueckner, G. E., et al. 1975, Sol. Phys., 45, 377
Shibata, K. 1999, Ap&SS, 264, 129
Tomczak, M. 1994, Ph.D. Thesis, Graduate Univ. of Wrocław, Wrocław
Tomczak, M. 1997, A&A, 317, 223
Tomczak, M. 2001, A&A, 366, 294
Tsuneta, S., Acton, L., Bruner, M., et al. 1991, Sol. Phys., 136, 37
Tsuneta, S., Hara, H., Shimizu, T., et al. 1992, PASJ, 44, L63
Uchida, Y., Fujisaki, K., Morita, S., et al. 1999, PASJ, 51, 53
Vaiana, G. S., Krieger, A. S., & Timothy, A. F. 1973, Sol. Phys., 32, 81
Vorpahl, J. A., Tandberg-Hanssen, E., & Smith, J. B. 1977, ApJ, 212, 550
Willingale, R. 1981, MNRAS, 194, 359